Parametric Study of Pulse-Combustor-Driven Ejectors at High-Pressure

Shaye Yungster[1]
Ohio Aerospace Institute, Cleveland, OH 44142

Daniel E. Paxson[2] and Hugh D. Perkins[3]
NASA Glenn Research Center, Cleveland, OH 44135

Pulse-combustor configurations developed in recent studies have demonstrated performance levels at high-pressure operating conditions comparable to those observed at atmospheric conditions. However, problems related to the way fuel was being distributed within the pulse combustor were still limiting performance. In the first part of this study, new configurations are investigated computationally aimed at improving the fuel distribution and performance of the pulse-combustor. Subsequent sections investigate the performance of various pulse-combustor driven ejector configurations operating at high-pressure conditions, focusing on the effects of fuel equivalence ratio and ejector throat area. The goal is to design pulse-combustor-ejector configurations that maximize pressure gain while achieving a thermal environment acceptable to a turbine, and at the same time maintain acceptable levels of NOx emissions and flow non-uniformities. The computations presented here have demonstrated pressure gains of up to 2.8%.

Nomenclature

D_{th}	=	Ejector throat diameter
EI	=	emission index (grams of NO per kilogram of fuel)
FASH	=	"fat and short" pulse-combustor configuration
f	=	pulse combustor operating frequency
$\dot{m}_f$	=	fuel massflow rate
$\dot{m}_{pri}$	=	primary massflow rate
$\dot{m}_{\sec}$	=	secondary massflow rate
$\dot{m}_{tot}$	=	total massflow rate
p	=	pressure
p_b	=	back pressure
p_0	=	inlet total pressure
PES	=	pule-combustor-ejector-shroud configuration
T	=	temperature
T_0	=	inlet total temperature
t	=	time
β	=	bypass ratio $(\dot{m}_{\sec}/\dot{m}_{pri})$
ϕ	=	equivalence ratio

[1] Senior Scientist, Senior AIAA Member.

[2] Aerospace Engineer, Associate Fellow AIAA.

[3] Aerospace Engineer, AIAA Member.

I. Introduction

Conventional gas turbine engines based on steady, constant pressure combustion actually result in total pressure losses that can range from 4 to 8 percent[1]. Typically, a one percent increase in total pressure loss can result in either a half percent reduction in thrust or a quarter percent increase in specific fuel consumption[1]. Efforts to overcome this limitation in conventional gas turbine engines has led to a large number of experimental and analytical investigations of unsteady pressure gain combustion concepts that include detonation based devices, wave rotors and resonant pulse combustors. This paper focuses on the pulse combustor concept and presents a computational study of an ejector based configuration, at high-pressure conditions, for application to gas turbine engines.

Pulse-combustors are unsteady, resonant thermo-acoustic devices in which heat released by combustion is coupled with the acoustic field. When used in combination with ejector systems, pulse-combustors have several advantages over alternative pressure gain combustion concepts. By being relatively simple devices, pulse-combustors avoid the mechanical complexities of higher pressure gain concepts such as wave rotors and detonation based devices. In addition, flow non-uniformities at the exit of pulse-combustor-ejector devices have been shown to be significantly lower than those observed in detonation-based devices[2]. This smoothing aspect of pulse-combustor-based systems is critical for maintaining high turbine performance. In addition, the emissions of oxides of nitrogen in pulse-combustors are potentially lower than in conventional combustor systems[3]. The main disadvantage of pulse-combustor-based systems is that the pressure-gain attainable is typically lower than that for wave rotors or detonation based devices.

Practical aerospace applications of pressure-gain combustion systems necessitate operation at high-pressure conditions. Preliminary calculations of pulse-combustors-ejector configurations operating at high-pressure conditions (10 bar) produced pressure gains significantly lower than those observed experimentally and computationally at atmospheric conditions[4]. A recent study[5] identified the factors limiting the pressure-gain at high-pressure conditions and investigated the effects of fuel injection and air mixing characteristics on performance. New pulse-combustor configurations were developed in Ref. 5 which were able to achieve performance levels at high-pressure conditions comparable to those observed at atmospheric conditions.

The study presented in Ref. 5 only considered the pulse-combustor by itself (i.e., without an ejector). However, the pulse-combustor by itself is not suitable to replace a conventional combustor in a gas turbine engine. This is because the pulse-combustor exhaust flow is too hot for a turbine to tolerate, and also because connecting a turbine directly downstream of the pulse combustor would completely disrupt the acoustic field and its coupling with the combustion process, an interaction that is critically important for the operation of pulse-combustors (see discussion in Refs. 4 and 5). Therefore, in practical applications the pulse-combustor must be combined with some type of ejector device.

The results obtained in Ref. 5 further revealed that two counter-rotating vortices were formed in the pulse-combustor, and that the fuel was being split between these two vortices. The combustion occurring in the secondary vortex, located further away from the combustor head-end, was not being confined as efficiently as the combustion occurring in the primary vortex, potentially affecting negatively the pressure gain in the combustor.

The first part of this paper (section 3.1) analyses various pulse-combustor configurations that attempt to address this issue. The remainder of the paper investigates the performance of various pulse-combustor-ejector configurations operating at high-pressure conditions, focusing on the effects of equivalence ratio and ejector throat area. The goal is to design pulse-combustor-ejector configurations that maximize pressure gain while achieving a thermal environment acceptable to a turbine, and at the same time maintain acceptable levels of NOx emissions and flow non-uniformities.

II. Computational Model

The pulse-combustor considered in this and our previous studies[4,5] is based on an experimental device investigated at the NASA Glenn Research Center[2]. Figure 1 shows a schematic of the experimental pulse-combustor and the axisymmetric computational model. The reed valve is the only moving part in the pulse-combustor. Its position is determined at every instant by the pressure differential existing between the inlet and combustor sides. To approximate the reed valve action, we use the vertically sliding, "reverse" valve model developed in our previous work[5]. In this model, the valve opens vertically from the bottom to the top of the inlet passage, and closes from top to bottom.This valve model removes the need to compute a special boundary condition at the combustor/inlet interface that has been used in previous studies[6,7]. The combustor/inlet interface becomes an interior domain in the CFD calculation, and a specified total pressure and total temperature boundary condition is applied upstream, at the inlet entrance (Fig. 1b). Opening and closing of the valve is determined by the pressure at the head-end of the pulse-combustor, and the motion of the valve as a function of time is specified by an exponential function. The other boundaries (Fig. 1b) were treated as either subsonic inflow, where the total pressure (p_0) and total temperature (T_0) were specified, or subsonic outflow, where the static pressure was imposed. In this study, the static pressure was set

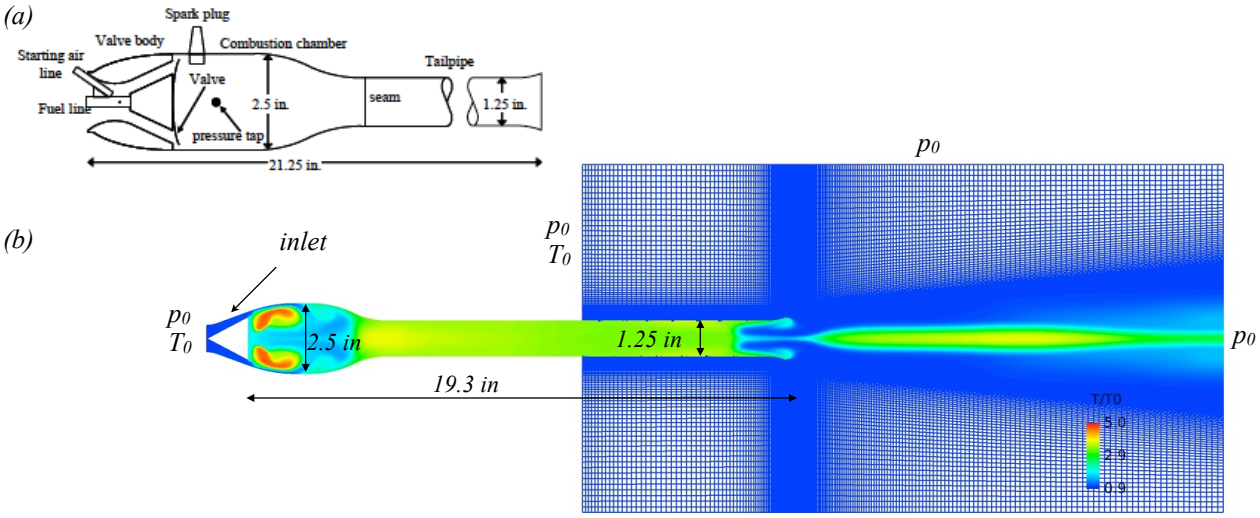

Figure 1. (a) Schematic of experimental pulse-combustor; (b) computational model.

equal to the total pressure p_0. Fuel is injected through discrete injectors located inside the inlet just upstream from the valve.

The numerical simulations of the pulse-combustor are carried out using a Computational Fluid Dynamics (CFD) code developed in-house[8,9]. The analysis is based on the axisymmetric, unsteady, Reynolds-averaged Navier-Stokes equations for a multi-species, thermally perfect, chemically reacting gas. The turbulence model used in the calculations is the Spalart-Allmaras one-equation model[10]. Adiabatic walls were assumed for all cases considered, and the grid had a minimum wall spacing of 1×10^{-3} in (resulting in values for y^+ of order one).

The numerical method used for solving the governing equations is described in detail in Refs. 8 and 9. Briefly stated, the equation set is solved using a fully implicit, variable-step backward differentiation formula (BDF) method. In this research, the temporally first order backward Euler version of the scheme was utilized. The numerical fluxes are evaluated using a second-order spatially accurate total variation diminishing (TVD) scheme. The resulting equations are then linearized in a conservative manner and solved iteratively, by using a lower-upper relaxation procedure consisting of successive Gauss-Seidel (LU-SGS) sweeps.

The fuel considered in this study is gaseous Jet-A, which is modeled as a $C_{11}H_{21}$ species. A reduced combustion mechanism, based on the model developed by Ajmani et al.[11,12], consisting of 10 elementary reactions among 11 reacting species was utilized. An extended Zeldovich mechanism for the computation of thermal NO production was added to the combustion model. The additional four NO reactions, were taken from Jachimowski's mechanism[13]. The complete reaction mechanism is given in Refs. 4 and 5.

III. Numerical Simulations

All the numerical simulations presented here were run for multiple cycles until the overall flowfield approached periodicity (limit cycle). This typically required 8-12 cycles for the pulse-combustor calculations (without an ejector), and up to 25 cycles for pulse-combustor-ejector configurations. The computational model that has been developed, permits the study of various configurations in multi-cycle mode within reasonable computational times. A typical case (170000 grid points) required 16 hours of wall-time per cycle using 24 processors on the NAS supercomputer "Endeavour".

All the cases presented in this paper consider inflow conditions of p_0 = 10 bar and T_0 = 550 K, which are representative of typical high-pressure gas turbine operation.

(3.1) Effect of geometric configuration on pulse-combustor performance (without an ejector)

In our recent study[5], which considered the pulse-combustor by itself (i.e., without the ejector), new pulse-combustor configurations were developed that demonstrated performance levels at high-pressure conditions comparable to those observed at atmospheric conditions. However, the results obtained in that study revealed potential problems related to the way fuel was being distributed within the pulse combustor. The results obtained in Ref. 5 showed that two counter-rotating vortices are formed in the pulse-combustor, and that the fuel was being split between these two vortices with nearly 60% of the fuel going into the secondary vortex (see Fig. 2a). There are

reasons to suspect that the combustion occurring in the secondary vortex, located further away from the combustor head-end, is not being confined as efficiently as the combustion occurring in the primary vortex. This confinement process in pulse combustors, achieved by the synchronized action of the heat release and the acoustic wave system, approximates constant volume combustion and is the mechanism by which pressure gain is achieved in these devices. If a large portion of the combustion process is not being confined efficiently the net pressure gain of the system could be affected negatively.

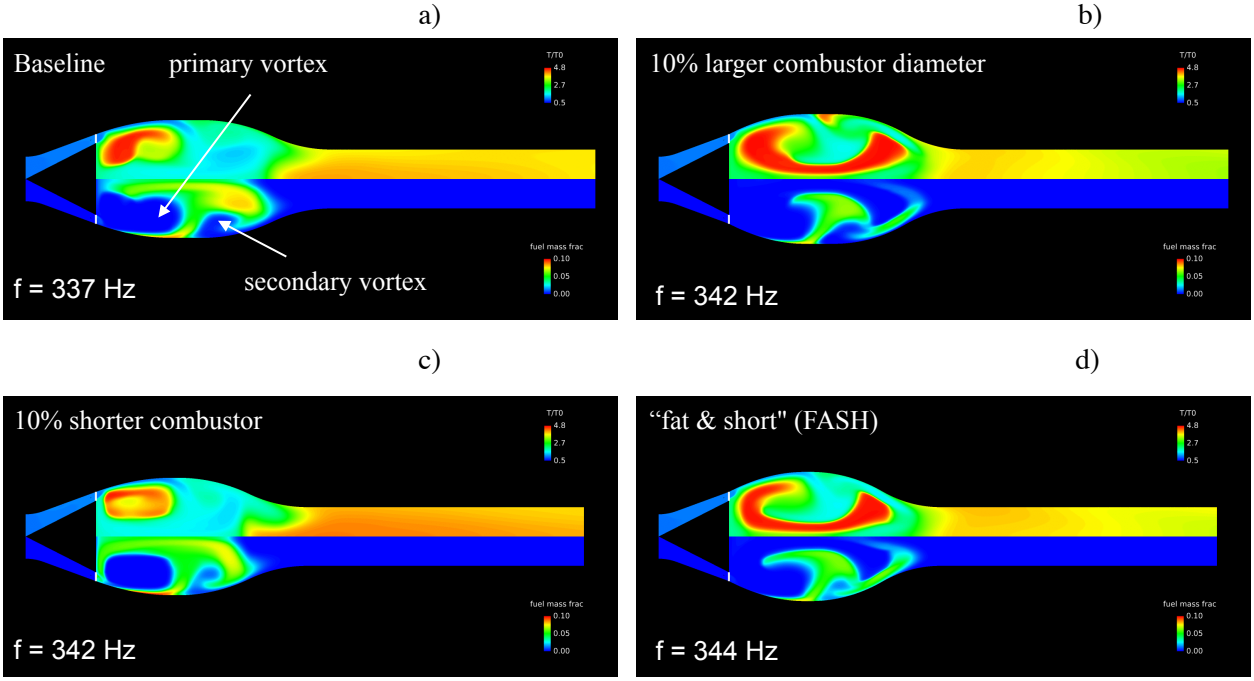

Figure 2. Temperature contours (top half) and fuel mass fraction contours (bottom half) at cycle start for four different pulse-combustor configurations; (a) baseline combustor; (b) 10% shorter combustor; (c) 10% larger combustor diameter; (d) shorter and larger diameter combustor (10%). ϕ **= 0.72.**

In an attempt to improve the fuel distribution in the pulse combustor we modified the baseline combustor by either reducing the combustor length or increasing the combustor diameter, and by combining these two modification into one additional configuration. The resulting four configurations that were analyzed are presented in Fig. 2.

All four cases were run at an equivalence ratio of ϕ = 0.72. Temperature contours are shown at the top half of each figure, and fuel mass fraction contours are shown at the bottom half, at the start of a pulse-combustor cycle (defined as the instant when the valve just finished closing). For clarity, only part of the pulse combustor tailpipe is shown. Figure 2 shows results for the baseline combustor (Fig.2a), a 10% shorter combustor (Fig.2b), a combustor with a 10% larger diameter (Fig.2c), and a combustor having both a 10% shorter length and larger diameter (“fat & short” or FASH configuration, Fig. 2d). This figure shows the effects of geometry on vortex structure, combustion dynamics and fuel distribution. These modifications also affect the pulse-combustor pressures and NOx emissions.

To further examine the effects of combustor geometry on the flow and combustion process, we compare in figures 3 and 4 the results obtained with the baseline and one of the modified pulse combustors, namely the FASH configuration. Figures 3 and 4 show temperature contours (top half) and fuel mass fraction contours (bottom half) during one cycle. Referring to Figs. 3a and 4a, which shows the flowfield just after the valve has fully closed, combustion is seen occurring mainly at the center of the primary vortex, however for the FASH configuration the flame has already propagated significantly throughout the combustor, consuming fuel in both the primary and secondary vortices. At the 0.5 ms mark, most of the fuel has been burnt in the FASH configuration while some unburnt fuel can still be seen in the baseline configuration. The valve begins to open at $t = 1.44$ *ms* and $t = 1.36$ *ms* respectively for the baseline and FASH configurations and air is seen entering the combustor in Figs 3d, 3e and 4d, 4e. The fuel injection process starts at $t = 2.24$ *ms* and $t = 2.16$ *ms* respectively for the baseline and FASH

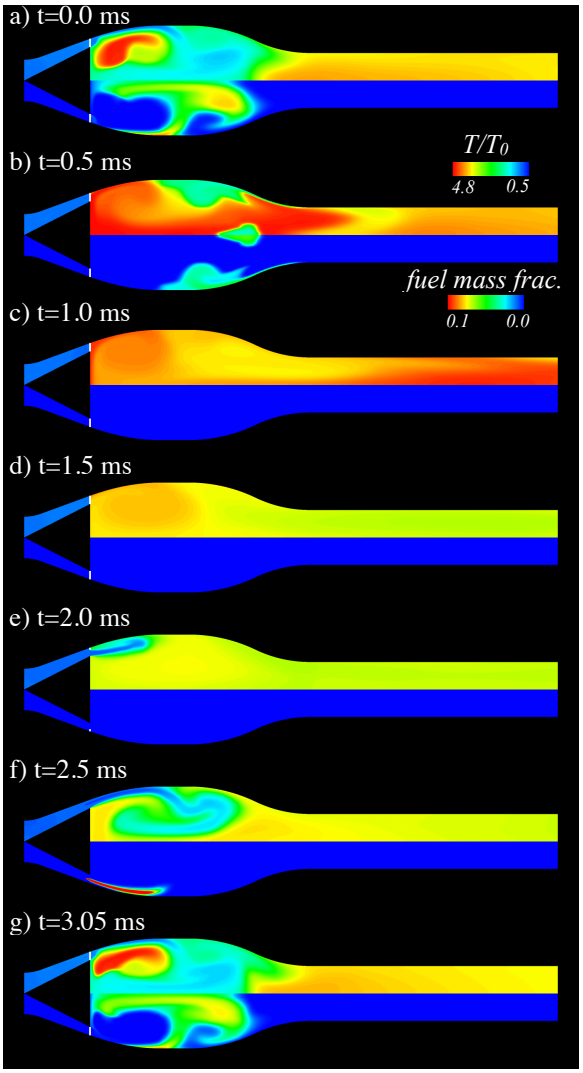

Figure 3. Temperature contours (top half) and fuel mass fraction contours (bottom half) at various times during one cycle (ϕ = 0.72). Baseline combustor.

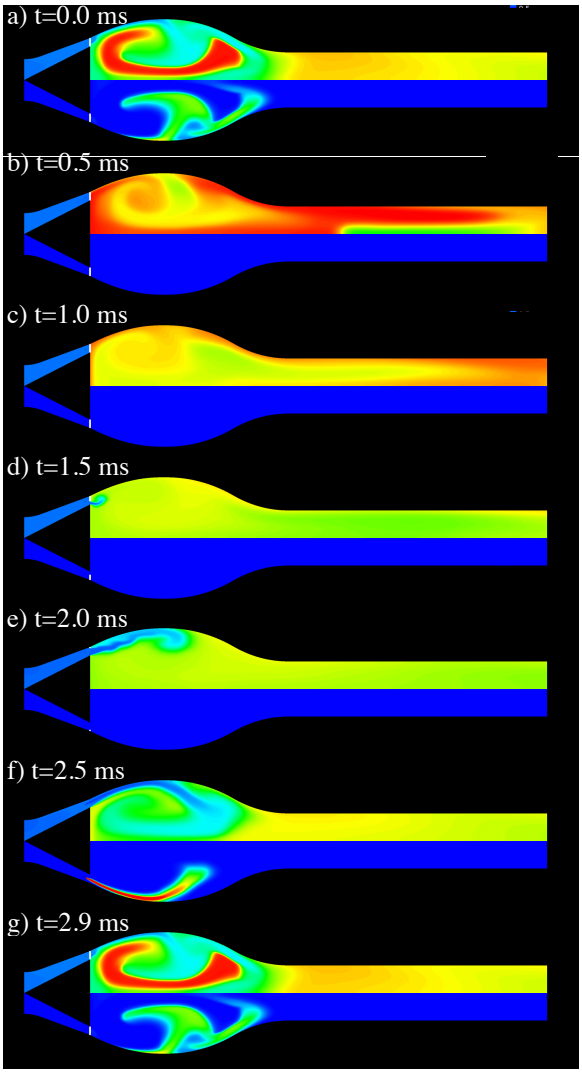

Figure 4. Temperature contours (top half) and fuel mass fraction contours (bottom half) at various times during one cycle (ϕ = 0.72). FASH combustor.

configurations and fuel is observed entering the combustor in Figs. 3f and 4f, which mixes with the incoming air and with the combustion products produced in the previous cycle. Subsequently, combustion begins at the vortex core (Figs. 3g and 4g) and the cycle repeats. Note that a much smaller fraction of the fuel reaches the secondary vortex in the FASH configuration compared with the baseline combustor.

The pressure histories at the head-end of the combustor, for the four pulse combustor configurations shown in Fig. 2, are plotted in Fig. 5. Note that the baseline case exhibits a period doubling behavior, i.e., the flow is periodic but repeats every other cycle. The three modified combustor configurations resulted in higher average combustor pressure compared with the baseline case. Increasing the combustor diameter resulted in higher pressure peaks but with a narrower profile. The shorter and FASH combustor configurations produced the highest average combustor pressure.

Figure 6 compares the emission index obtained with the four combustor configurations. This figure plots the emission index computed at the entrance and exit of the pulse-combustor tailpipe, showing that most of the NO is produced in the combustor. The results indicate that the three modified combustor configurations produce between 40% and 50% more NO than the baseline configuration. Therefore, the higher average combustor pressures appear to be a achieved at a cost of higher NO production.

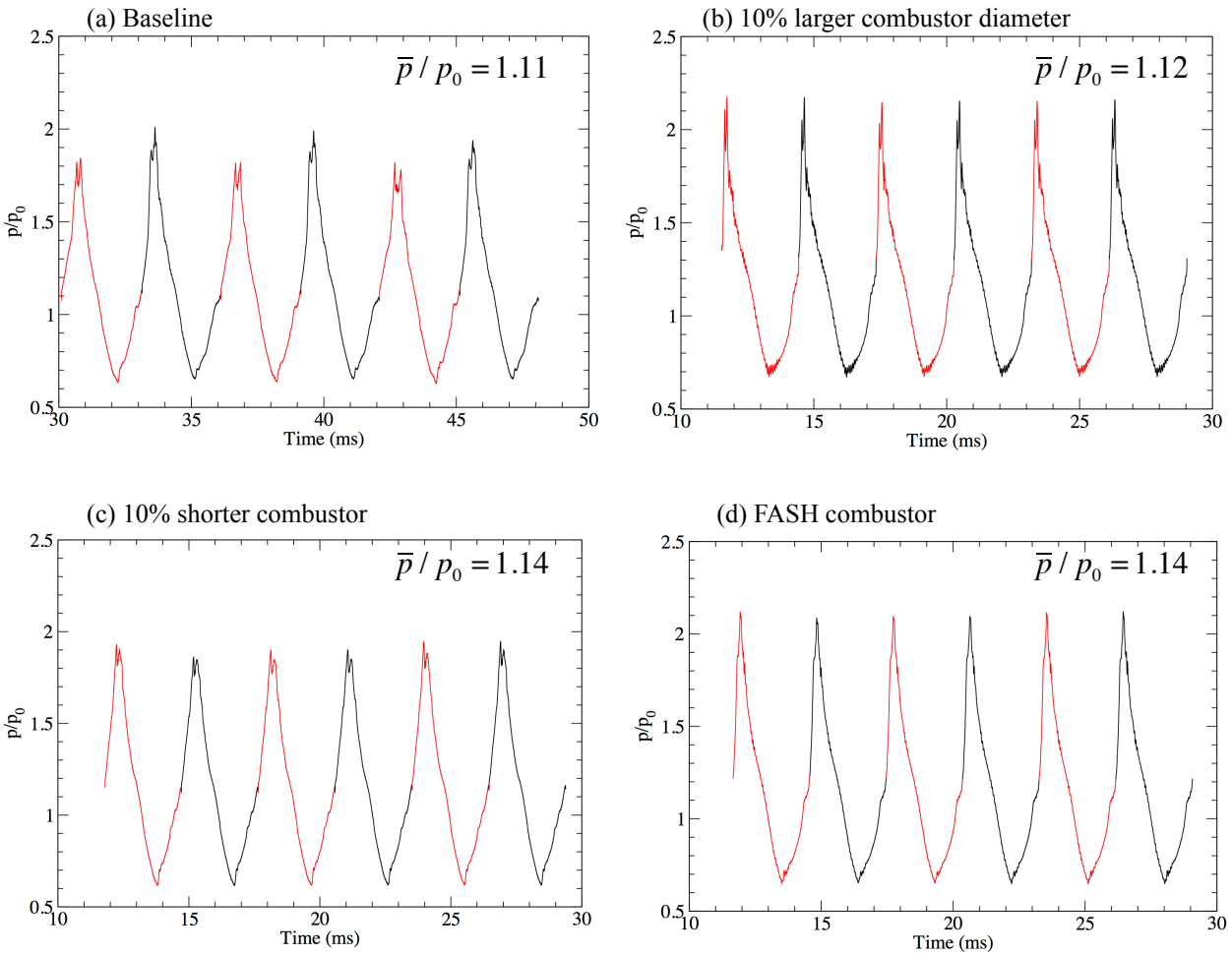

Figure 5. Pressure vs time for four pulse-combustor configurations. (ϕ = 0.72).

It is also apparent from Fig. 6 that a larger fraction of the total NO is being produced in the combustor tailpipe for the three modified configurations than for the baseline configuration. For the baseline case, 12% of the NO is produced in the tailpipe, while for the modified cases it's 20%, 26% and 31% respectively. One possible explanation for this result is that in the baseline case, a large fraction of the fuel ends up in the secondary vortex, where confinement of the combustion process is less efficient and therefor, the residence time of the combustion products at the high combustion temperature is shorter. This in turn results in lower NO production. The levels of NO emissions from all four pulse combustor configurations, however, are comparable to those obtained with conventional gas turbine engines operating at corresponding compressor pressure ratios (see Fig. 23 in Ref. 4).

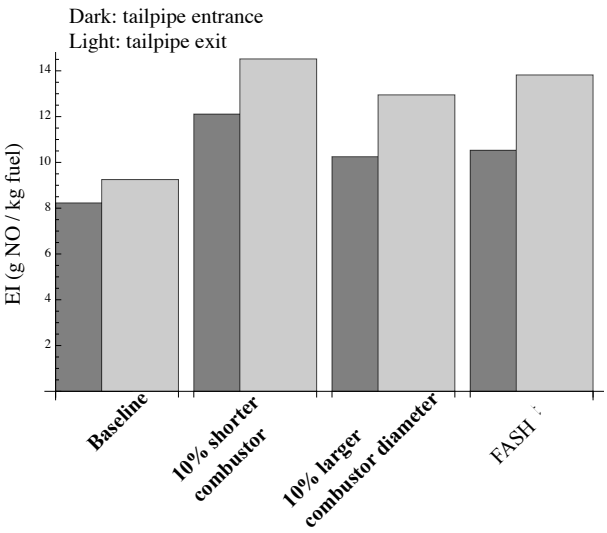

Figure 6. Emission index results for four combustor

(3.2) Analysis of the FASH pulse-combustor-ejector configuration.

The FASH pulse combustor configuration resulted in high average pressure levels and moderate NO production, and therefore was selected for analysis in combination with an ejector. The pulse-combustor-ejector configuration considered in this study is based on the experimental device tested by Paxson and Dougherty[2]. They combined a pulse-combustor with an ejector and housed both within a shroud. Their study showed that such a device could achieve a pressure gain of 3.5% at an overall temperature ratio commensurate with modern gas turbines. The resulting pulse-combustor-ejector-shroud (PES) configuration is shown in Fig. 7. A similar configuration was analyzed in our earlier computational study[4]. The ejector has a 6.0 in diameter and its throat is located 4.0 in

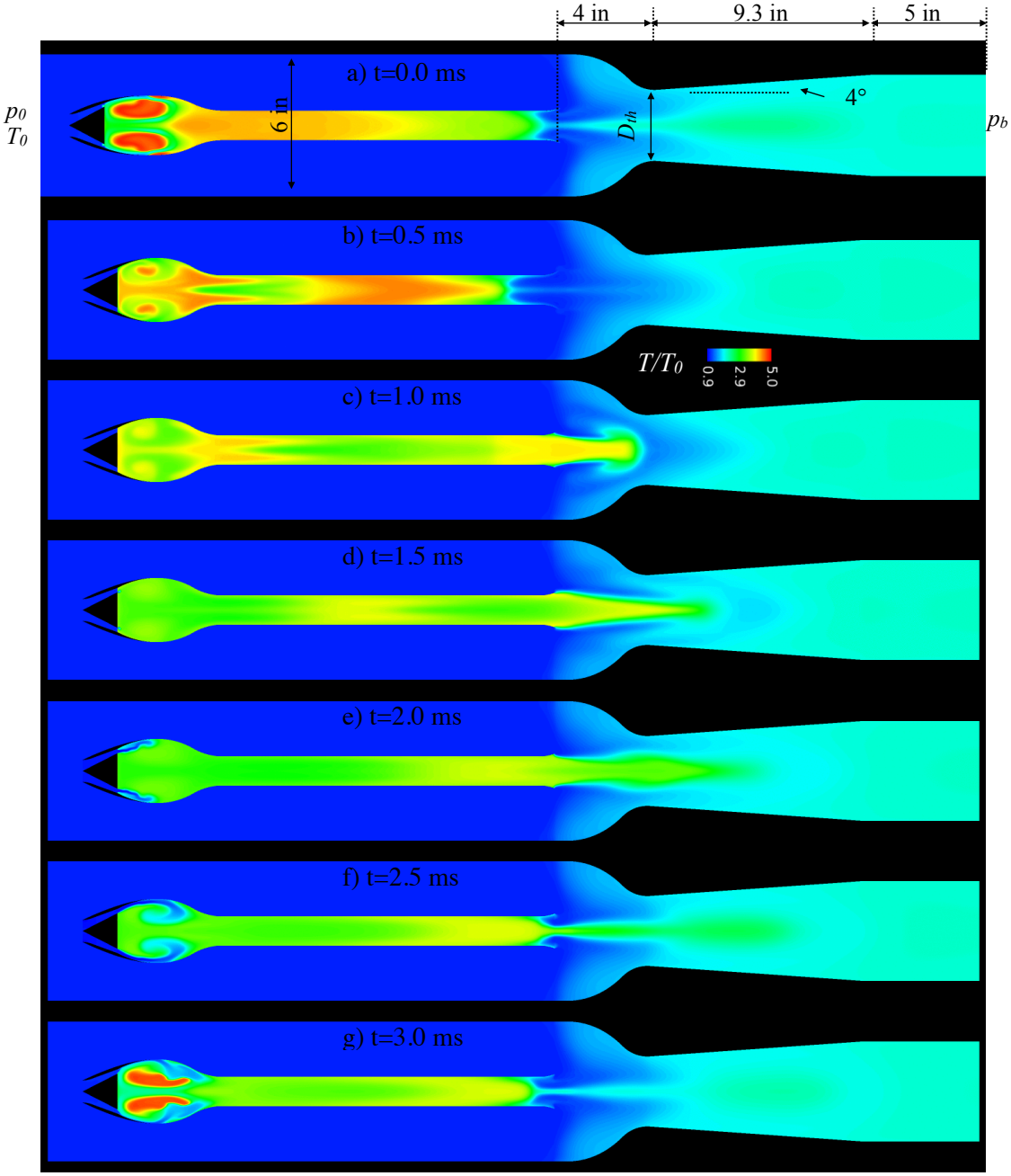

Figure 7. Temperature contours at various times during one cycle for a PES combustor based on the FASH configuration (ϕ = 0.67).

downstream from the end of the pulse-combustor tailpipe. At the inflow plane of the computational domain, a specified total pressure and total temperature boundary condition is imposed. As in the case of the pulse-combustor by itself, all ejector cases presented in this paper are based on p_0 = 10 bar and T_0 = 550 K. The air entering the PES combustor is split into two streams. The primary stream flows through the pulse-combustor while the secondary stream bypasses it. The two streams interact and mix in the ejector. At the exit plane of the PES combustor a fixed static pressure , p_b, boundary condition is imposed.

One of the main objectives of this study is to determine the pressure gain attainable across the PES combustor without exceeding the maximum temperature allowed by a turbine. Specifically, we look for the mass-averaged temperature at the exit of the PES combustor to be around two times the inlet total temperature, or 1100 K. The back pressure and the pumping action of the pulse-combustor determine the total airflow through the engine, and therefore will also determine the exit temperature. The pressure gain is defined here as the difference between the mass-averaged total pressure ratio at the exit and the inflow total pressure ratio (expressed as a percentage).

Figure 7 shows temperature contours at various times during one cycle. The ejector in this case had a throat diameter of , D_{th}, = 3.0 in, and the back pressure, p_b, was set to p_b = (1.017)p_0. The fuel injection pressure, timing and duration was kept identical to the case of the pulse combustor by itself (Fig.4). The additions of the ejector and the back pressure imposed on the system had a significant impact on the pulse-combustor flowfield. Comparing Figs. 4 and 8, it is evident that the combustion pattern has changed. Also the primary airflow through the combustor is approximately 10% lower in the PES configuration ($\bar{m}_{pri} = 0.230$) compared with the pulse combustor by itself ($\bar{m}_{pri} = 0.256$). The fuel flow is also lower in the PES configuration resulting in a lower equivalence ratio ((ϕ = 0.67) than the pule-combustor by itself case (ϕ = 0.72). The bypass ratio for this case was $\beta = \bar{m}_{sec} / \bar{m}_{pri} = 1.91$.

Other changes in the overall flowfield are also apparent. Figure 8 shows the pressure history at the head-end of the combustor. The pressure history now exhibits a period-tripling behavior, i.e., the flow is periodic but repeats itself every third cycle. In comparison, the pressure profile for the pulse combustor alone shows a uniform profile for every cycle (Fig. 5d). The average combustor pressure ratio is slightly lower (1.12 vs 1.14) and the average frequency is slightly higher (353 Hz vs 344 Hz), although the frequency for each individual cycle varies from 332 Hz to 395 Hz.

Figure 9 shows the mass-averaged total temperature and total pressure computed at the exit plane of the PES combustor for several cycles. Note that It takes more than 20 cycles for the solution to converge. The exit mass-averaged temperature was around 1130 K, close to our target value of 1100 K. The pressure plot indicates a pressure gain of approximately 2.4%, twice the value obtained in our initial (and preliminary) study[4].

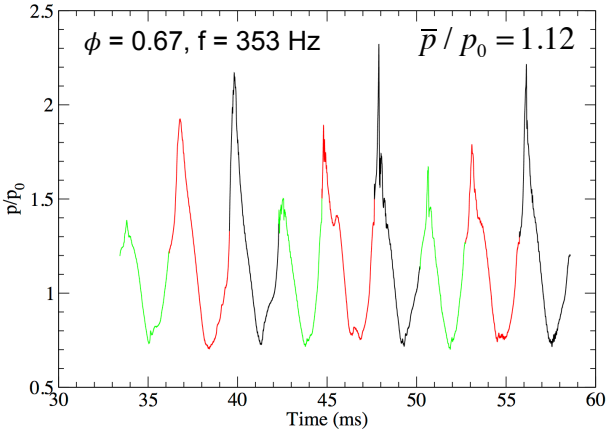

Figure 8. Pressure vs time for the PES combustor based on the FASH configuration . (ϕ = 0.67).

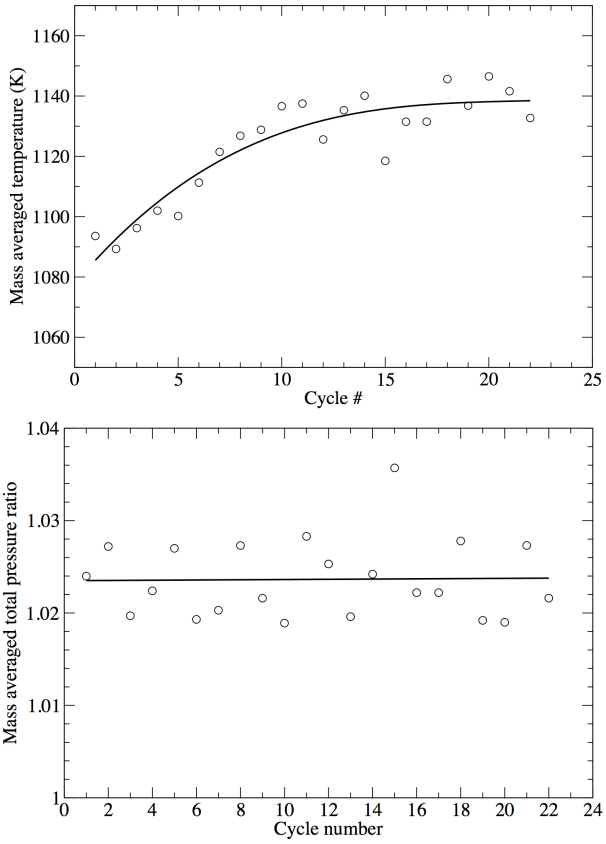

Figure 9. Mass-averaged total pressure and total temperature at the exit of the PES combustor (FASH configuration).

(3.3) Effect of equivalence ratio on the baseline PES combustor

We investigated the effects of equivalence ratio on the performance of a PES combustor derived from the baseline configuration (Fig. 2a). We computed three cases having equivalence ratios, ϕ, of 0.77, 0.83 and 0.90. The back pressure for all cases was set at $p_b = (1.017)p_0$.

Figure 10 shows pressure histories at the combustor head-end for the three cases. The pressure profile remains nearly unchanged when ϕ, is increased from 0.77 to 0.83, and the frequency of operation increases only slightly from 372 Hz to 378 Hz. Further increase to ϕ = 0.90 brings significant changes to the flowfield. The periodicity switches from triple period to single period. The peak pressures are significantly lower, but the average pressure remains nearly unchanged. The frequency of operation increases further to 387 Hz. The change in periodic behavior of the flowfield could be due to the increase in operating frequency which in turn alters the interaction with the acoustic field.

The bypass ratio for the two lower equivalence ratio cases was $\beta = 2.11$, and it decreased to $\beta = 1.89$ for the ϕ = 0.9 case. The primary mass flow rate decreased slightly for the ϕ = 0.9 case (from 0.19 to 0.18 kg/s).

Figure 11 shows the mass-averaged total temperature and total pressure computed at the exit plane of the PES combustor for the three cases. It can be seen that it takes between 12 and 25 cycles, depending on the particular case, for the mass-averaged temperature to converge. As the amount of fuel is increased, the mass-averaged temperature increases but the pressure gain remains nearly constant at around 2%. The only effect of a higher ϕ is to increase the temperature of the exhaust flow.

Since the bypass ratio for the ϕ = 0.77 and ϕ = 0.83 did not change, it is possible to do a quick estimate of the expected temperature increase in the exhaust flow caused by this change in ϕ. The analysis is presented in the appendix. The expected increase in temperature from this analysis was $\Delta T_e = 49.4$ K. From Fig. 11d, the computed temperature increase is approximately $\Delta T_{CFD} = 45$ K, in close agreement with the analytical value.

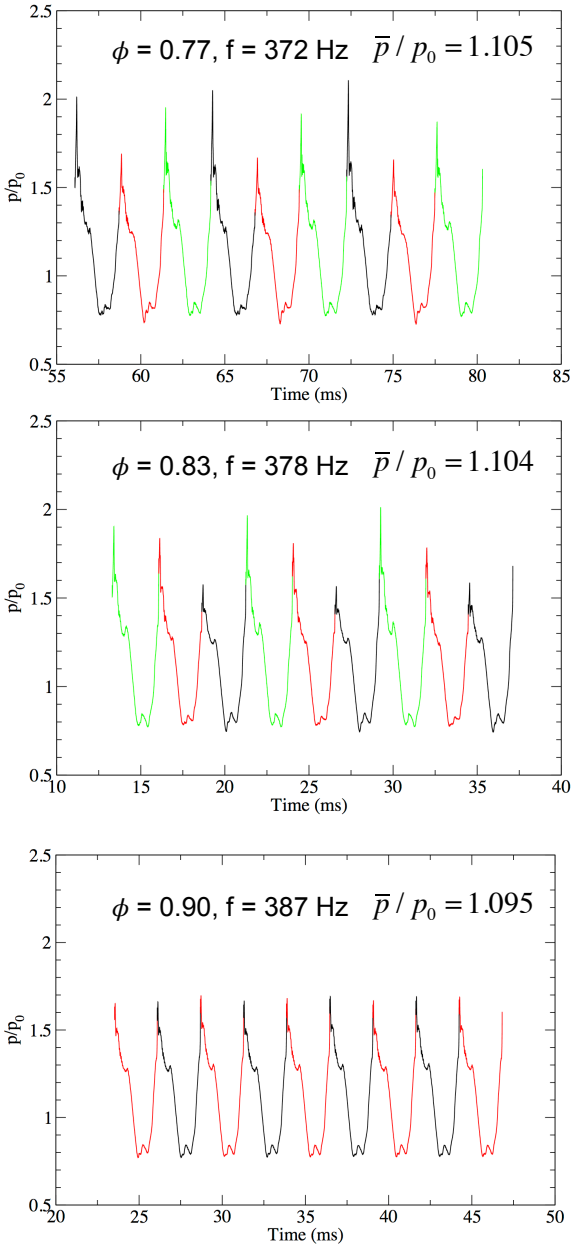

Figure 10. Pressure history for baseline PES combustor for three different equivalence ratios.

(3.4) Effect of ejector throat area on performance for baseline PES combustor.

We carried out an investigation of the effects of ejector throat area on the performance of the baseline PES combustor. Four ejectors were considered having throat diameters of 3.3 in, 3.0 in, 2.7 in and 2.4 in. Figure 12 shows temperature contours at the start of the cycle for the four configurations. In these calculations, the back-pressure was varied for each case in such a way as to obtain the desired mass-average temperature of 1100 K at the exit of the device. Indicated in Fig. 12 is the back-pressure that was used in each case. Note that the required back-pressure increases as the throat diameter (area) is decreased. This is due to the fact that as the throat diameter is decreased, the bypass airflow increases for a given level of back-pressure. Therefore, in order to obtain the desired exit temperature of 1100 K, a higher back-pressure can be imposed (which reduced the bypass airflow). Note also

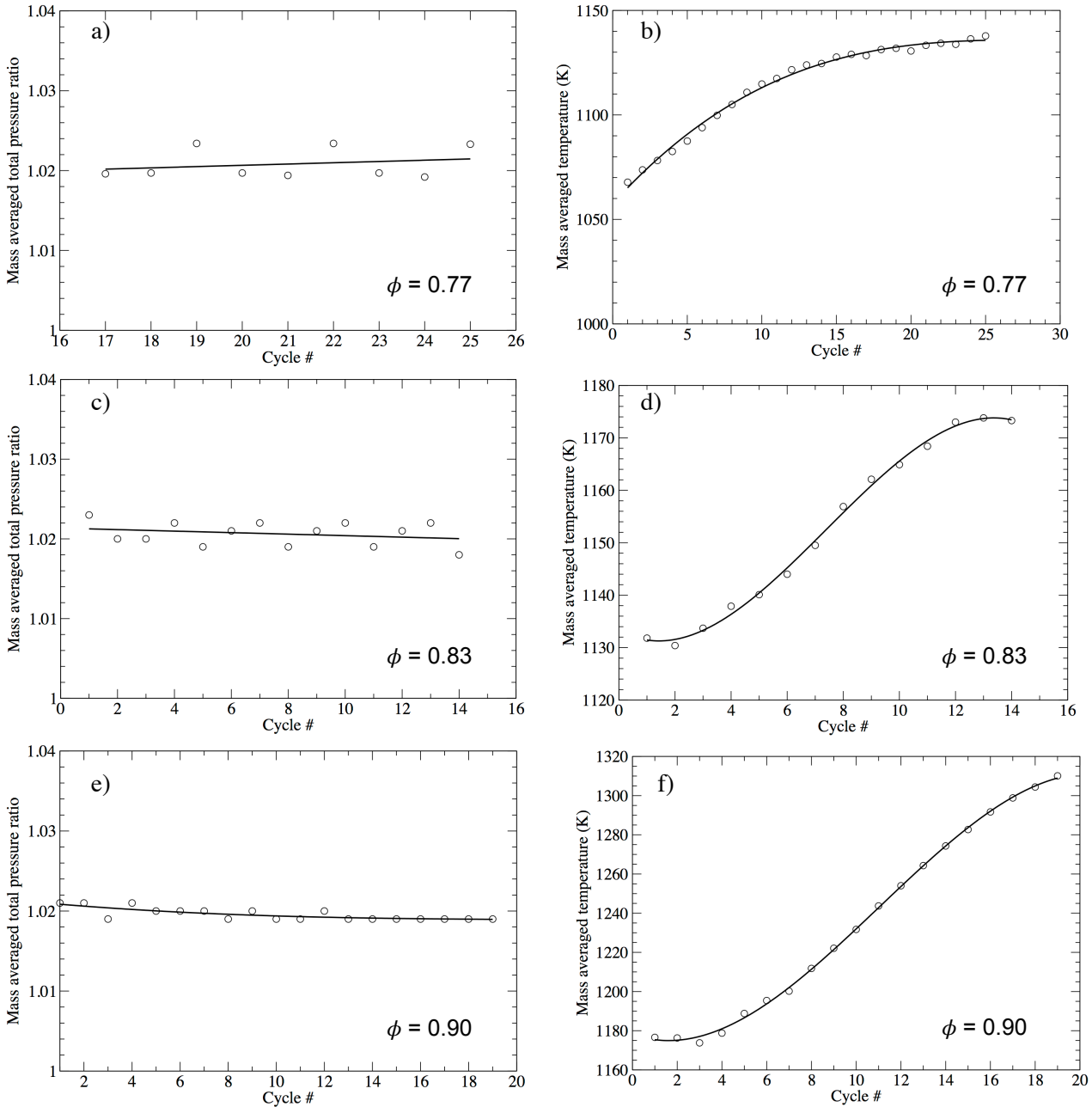

Figure 11. Mass-averaged total pressure and total temperature at the exit of the baseline PES combustor for three equivalence ratios..

that the structure of the combustion process is not significantly affected by the changes in the ejector configuration, however the reverse backflow into the pulse-combustor penetrates further into the tailpipe as the ejector throat diameter is decreased. This is an indication of a more effective performance of the pulse combustor resulting in a better pumping action. The average frequency of operation for all four cases was 372 Hz.

Figure 13 shows the pressures at the combustor head-end for the four ejector configurations. The average combustor pressure remains nearly constant for all cases, however there is a noticeable decrease in the peak pressure fluctuations from cycle to cycle as the throat diameter is decreased. This is particularly apparent for the $D_{th} = 2.4$ in case.

Figure 14 shows temperature (top half of each figure) and pressure (bottom half) contours at various times during one cycle for the $D_{th} = 2.4$ in case. The figure shows the pressure changes inside the pulse combustor that

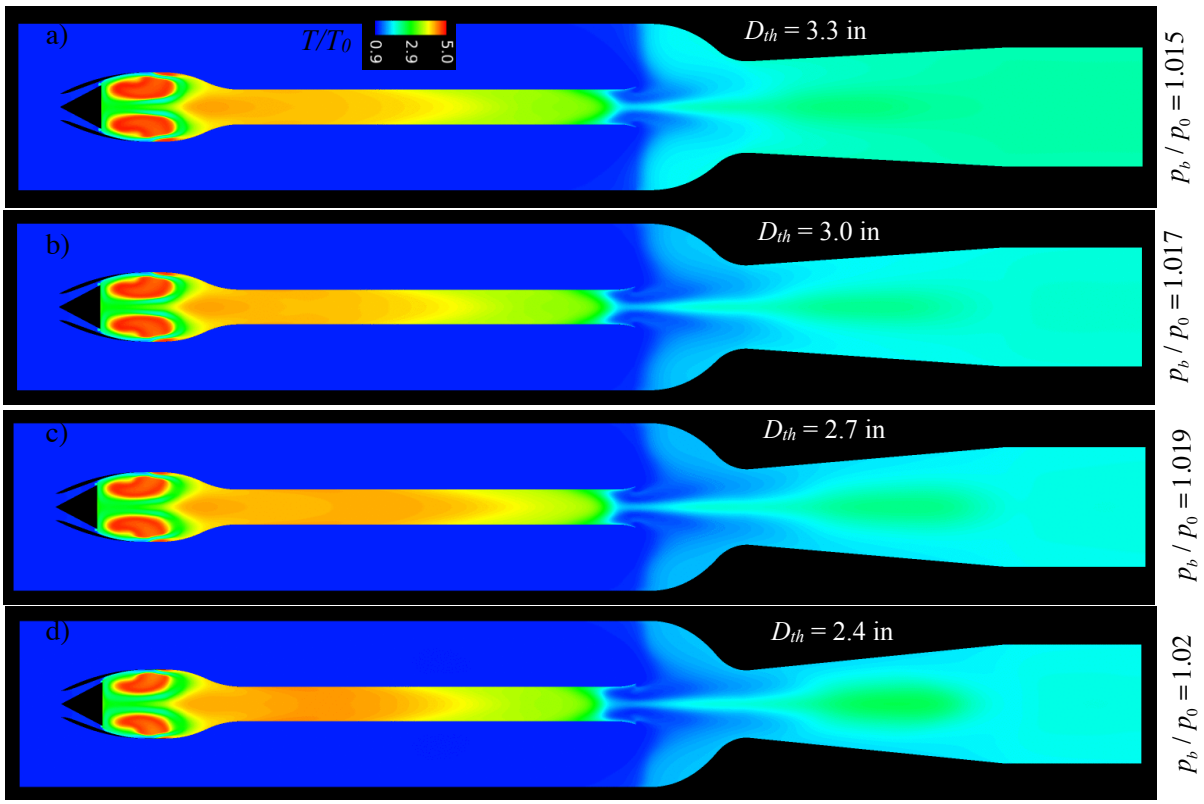

Figure 12. Temperature contours for four baseline PES combustor ejector configurations; (a) ϕ = 0.75, β = 1.47; (b) ϕ = 0.77, β = 2.11; (c) ϕ = 0.77, β = 2.40; (d) ϕ = 0.78, β = 2.59.

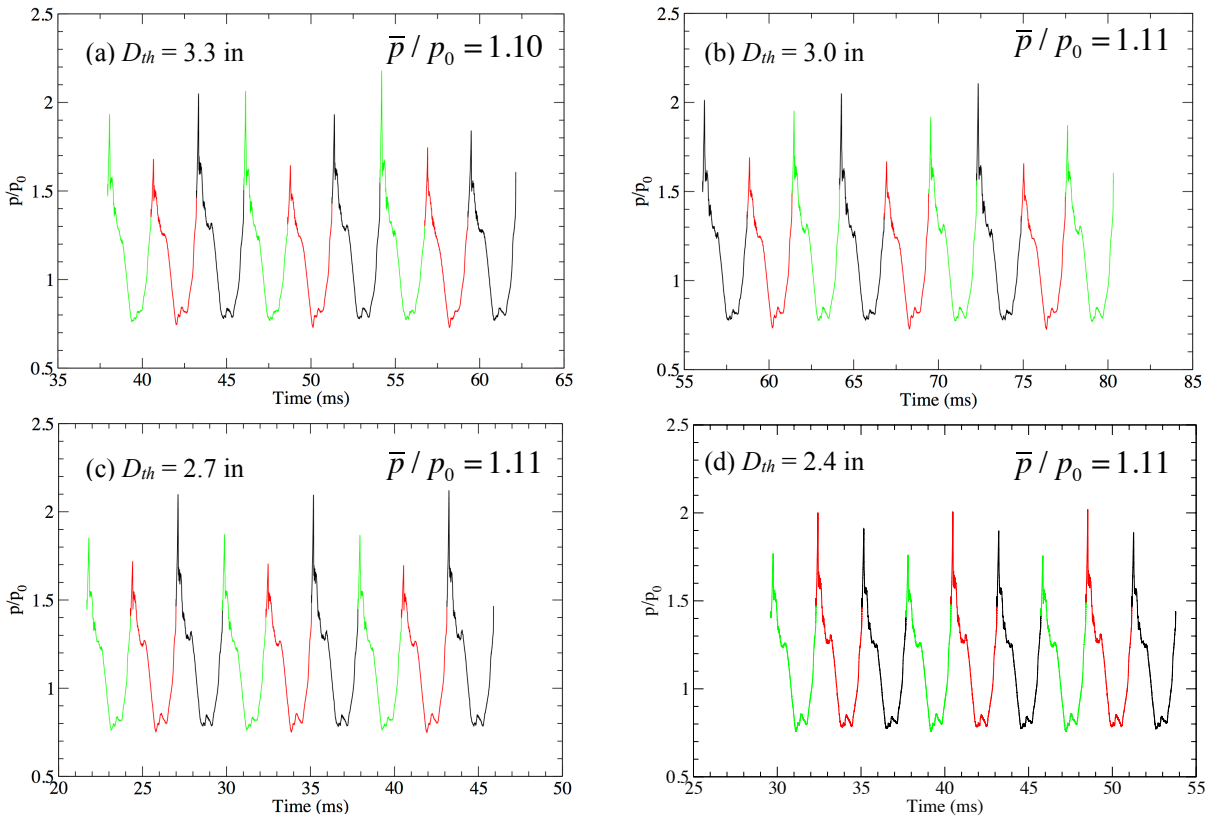

Figure 13. Pressure history for four baseline PES combustor configurations

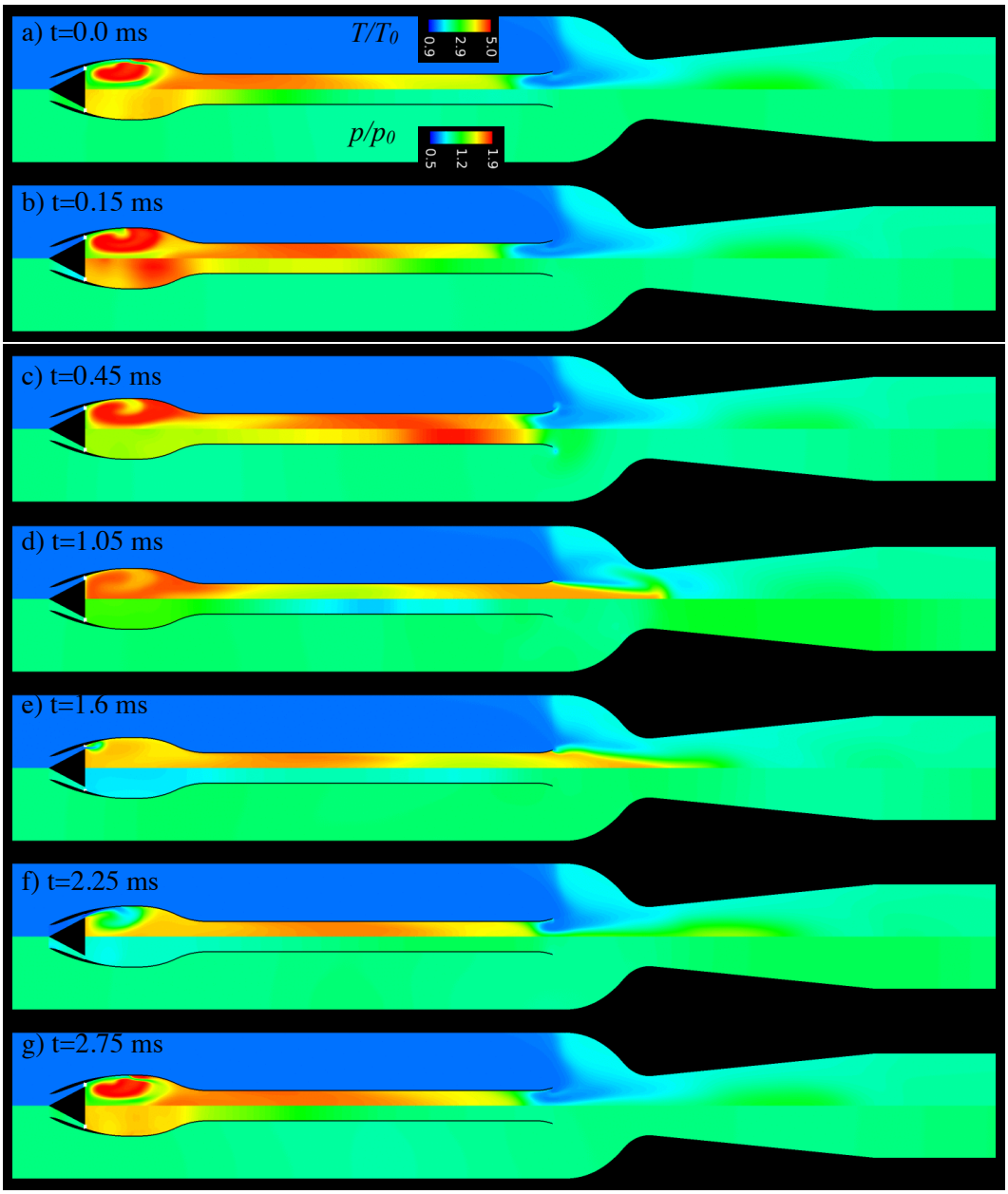

Figure 14. Temperature contours (top half) and pressure contours (bottom half) for the D_{th} = 2.4 in PES combustor configuration

occur during one cycle. The combustion process raises the temperature and pressure in the combustor and generates a reaction shock that propagates downstream (Figs. 14a-14c). When the reaction shock reaches the the end of the pulse-combustor, it is reflected as an expansion wave that propagates upstream (Fig. 14d). When the pressure in the combustor drops below the inlet pressure, the valve opens allowing air into the combustor (Fig. 14e, 14f). The expansion wave travels up and down the pulse-combustor length, and is reflected back as a compression wave at the pulse combustor exit. When this compression wave reaches the combustor it causes the pressure to rise and the valve to close (Fig. 14g).

Figure 15 shows the mass-averaged total pressure and total temperature computed at the exit of the PES combustor for the four ejector configurations. For the largest throat diameter case, the total pressure gain is slightly under 2% and the mass-averaged temperature is around 1240 K, higher than the target value. This result implies that for this case, the back-pressure imposed was too large and the bypass airflow was too low. For this case, the back-

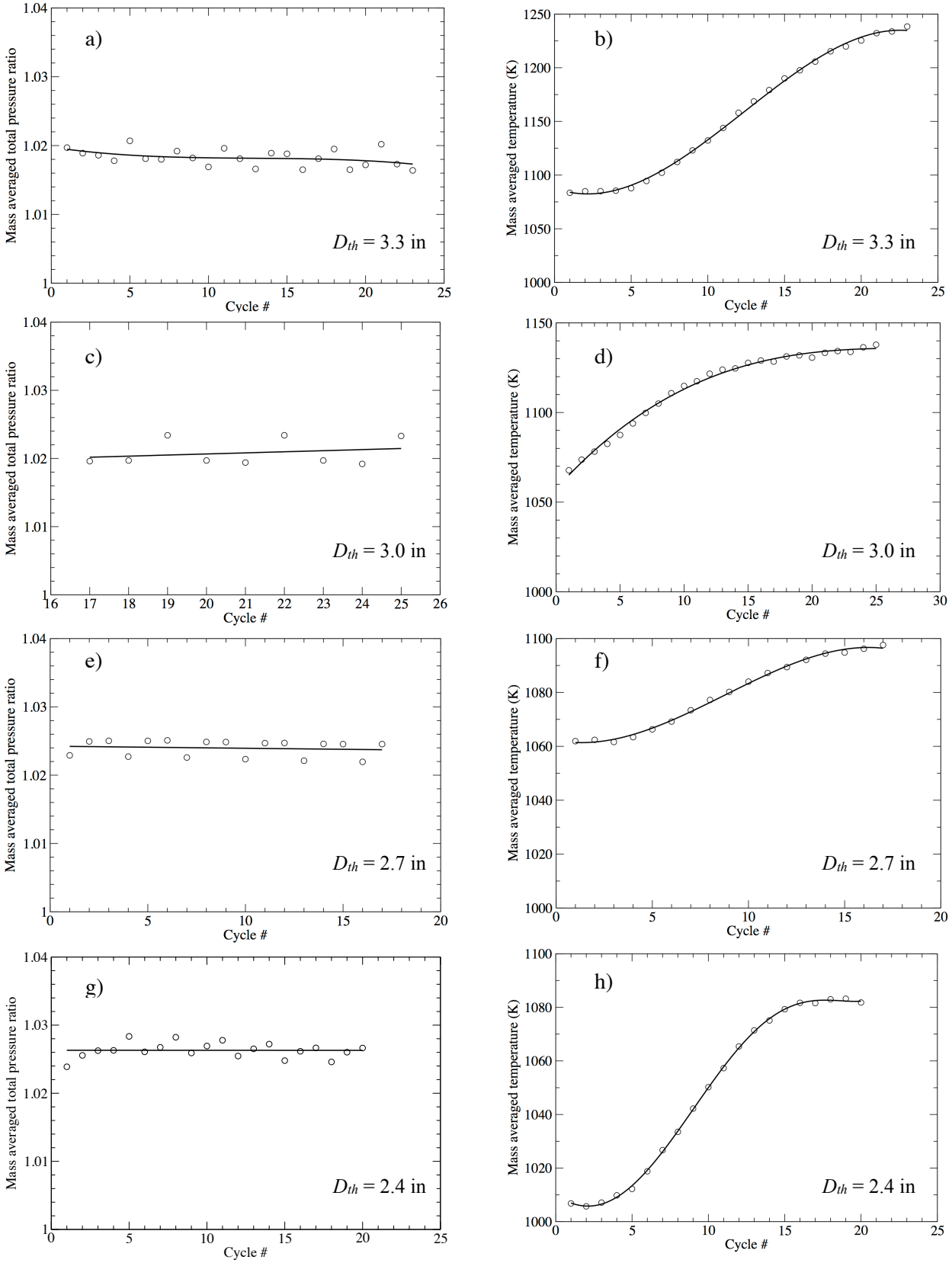

Figure 15. Mass-averaged total pressure and total temperature at the exit of the PES combustor for four ejector configurations.

pressure should have been reduced in order to increase the airflow. However, such an action would have also resulted in a lower pressure gain. For the other three configurations, the mass-averaged temperature was near the target value of 1100 K. As the throat diameter was decreased, the performance of the system increased which allowed a higher back-pressure to be imposed. Therefore, the pressure gain of this PES combustor configuration increases inversely proportional to the throat area. The highest pressure gain of ~2.8% was obtained with the smallest throat area.

The exact mechanism by which the performance of the PES combustor improves with a reduction in the ejector throat area is still being investigated. One key factor appears to be the fact that as the throat area decreases, the velocity increases, and more importantly, the pressure around the throat and around the pulse-combustor tailpipe exit decreases. Such low pressures at the exit of the pulse-combustor are beneficial for its efficient operation.

The case plotted in Fig. 15c and 15d for the baseline PES combustor correspond to the same ejector configuration as that shown in Fig. 7 for the FASH based PES combustor. The pressure gain for the FASH based PES combustor was ~2.4% (see Fig. 9) compared to ~2% for the baseline PES combustor (see Fig. 15c). Therefore, we expect that the FASH configuration combined with a smaller throat area ejector will produce a pressure gain higher than that shown in Fig. 15g. Such simulation is currently being carried out.

At this point, the optimum ejector throat area (and its location relative to the pulse combustor) has not been determined. The results presented here indicate that the smaller the throat area, the higher the pressure gain potential. At some point, further reductions in ejector throat area will begin to interfere with the pulse combustor operation and the performance of the system will decrease. Current studies are attempting to identify the optimal ejector configuration.

V. Conclusions

Pulse-combustor configurations recently developed were able to demonstrate performance levels at high-pressure operating conditions comparable to those observed at atmospheric conditions. However, problems related to the way fuel was being distributed within the pulse combustor were still limiting performance. The first part of this study, analyzed new pulse-combustor configurations that were aimed at improving the fuel distribution in the pulse-combustor. The new configurations were shown to produce higher average combustor pressures than the baseline case. The higher pressures, however, were achieved at the cost of higher NO production. The emission index levels for all cases where, nonetheless, comparable to those achieved in conventional gas turbine engines.

The pulse-combustor by itself, however, is not suitable to replace a conventional combustor in a gas turbine engine, because the pulse-combustor exhaust flow is too hot for a turbine to tolerate, and also because connecting a turbine directly downstream of the pulse-combustor would disrupt the coupling between the combustion process and the acoustic field. In practical applications the pulse-combustor must be combined with some type of ejector device.

The performance of various pulse-combustor driven ejector configurations operating at high-pressure conditions were investigated computationally, focusing on the effects of fuel equivalence ratio and ejector throat area. The goal was to design PES combustor configurations that maximize pressure gain while achieving a thermal environment acceptable to a turbine, and at the same time maintaining acceptable levels of NOx emissions and flow non-uniformities.

The effects of ejector throat area were particularly strong on the performance of the PES combustor. The pressure gain of the PES combustor configuration increased inversely proportional to the throat area. The highest pressure gain of ~2.8% was obtained with the smallest throat area considered. The exact mechanism by which the performance of the PES combustor improves as the ejector throat area decreases is still being investigated. However, one key factor appears to be the fact that as the throat area decreases, the pressure immediately downstream of the pulse-combustor tailpipe exit also decreases. The low pressure at the exit of the pulse-combustor provides a favorable boundary condition that appears to improve the overall performance of the system.

Based on the results presented, higher pressure gains are likely achievable by combining the FASH-based PES combustor with the 2.4 in throat diameter ejector. Such calculations are currently being carried out. The optimal ejector throat area and its location relative to the pulse-combustor has not yet been determined, and is the subject of current research.

Appendix

Here we present a quick estimate of the expected change in the temperature of the flow exiting the PES-combustor-as a result of an increase in the equivalence ratio in the pulse-combustor. The analysis assumes that the overall mass flow rate through the engine is not changed by the additional fuel.

A change in pulse-combustor equivalence ratio from ϕ_1 to ϕ_2, corresponds to the following additional fuel:

$$\frac{\Delta \dot{m}_f}{\dot{m}_{pri}} = \Delta\phi (f/A)_{stoich} \tag{1}$$

where $(f/A)_{stoich}$ is the stoichiometric fuel-air ratio. Then we can write:

$$\Delta \dot{m}_f Q^R = \dot{m}_{tot} c_p \Delta T \tag{2}$$

where Q^R is the heating value of the fuel. Therefore,

$$\frac{\Delta \dot{m}_f}{\dot{m}_{pri}} Q^R = \frac{\dot{m}_{tot}}{\dot{m}_{pri}} c_p \Delta T = (1+\beta) c_p \Delta T \tag{3}$$

and the expression for the increase in temperature of the flow exiting the PES combustor is given by

$$\Delta T_e = \frac{(\frac{\Delta \dot{m}_f}{\dot{m}_{pri}}) Q^R}{(1+\beta) c_p} \tag{4}$$

For Jet-A fuel we have:

$$(f/A/)_{stoich} = 0.06859 \tag{5}$$

$$Q^R = 43.5 \times 10^6 \ \text{J/Kg}_\text{f} \tag{6}$$

For the case considered at the end of section (3.3) relative to the results shown in Figs. 11b and 11d, the increase in equivalence ratio was $\Delta\phi = 0.06$ (increase from $\phi_1 = 0.77$ to $\phi_2 = 0.83$). Therefore, from equations (1) and (5):

$$\frac{\Delta \dot{m}_f}{\dot{m}_{pri}} = 4.115 \times 10^{-3} \tag{7}$$

Since the main component of the gas exiting the PES combustor is air, we can approximate the specific heat as that of air. For the case considered in section (3.3), the temperature at the exit is around 1100 K which results in a specific heat value of $c_p = 1.164$ KJ/Kg K.

The bypass ratio for this case was $\beta = 2.11$. Inserting these values into equation (4) gives the increase in temperature at the exit of the PES combustor:

$$\Delta T_e = 49.4 \ \text{K}. \tag{8}$$

Acknowledgments

This study was supported by NASA under contract number NNC13TA84T.04. The computational resources were provided by the NASA Advanced Supercomputing (NAS) Division.

References

1. Lefebvre, A.H., *Gas Turbine Combustion*, 2nd ed.,Taylor & Francis, Philadelphia,1998, Chapt. 4.
2. Paxson, D.E. and Dougherty, K., "Ejector Enhanced Pulsejet Based Pressure Gain Combustors: An Old Idea With a New Twist," AIAA paper 2005-4216, July 2005.
3. Keller, J.O. and Bramlette, T.T., "Pulse Combustion: The Importance of Characteristic Times," Combustion and Flame, 75, 33-44 (1989).
4. Yungster, S., Paxson, D.E. and Perkins, H.D.," Computational Study of Pulsejet-Driven Pressure Gain Combustors at High-Pressure," AIAA paper 2013-3709, July 2013.
5. Yungster, S., Paxson, D.E. and Perkins, H.D.," Effect of Fuel Injection and Mixing Characteristics on Pulse-Combustor Performance at High-Pressure," AIAA paper 2014-3728, July 2014.
6. Geng, T., Kiker Jr, A., Ordon, R., Kuznetsov, A.V., Zeng, F. and Roberts, W.L., "Combined Numerical and Experimental Investigation of a Hobby-Scale Pulsejet," Journal of Propulsion and Power, Vol. 23, No. 1, 2007.
7. Geng, T., Zheng, F., Kuznetsov, A. V., Roberts, W. L., Paxson, D. E., "Comparison Between Numerically Simulated and Experimentally Measured Flowfield Quantities Behind a Pulsejet, Flow," Turbulence and Combustion, Vol. 84, No. 4, pp. 653-667, May 2010.
8. Yungster, S. and Radhakrishnan, K., A Fully Implicit Time Accurate Method for Hypersonic Combustion: Application to Shock-Induced Combustion Instability. Shock Waves, 5, 293-303, (1996).
9. Yungster, S. and Radhakrishnan, K., Pulsating one-dimensional detonations in hydrogen-air mixtures. Combustion Theory and Modeling, 8, 745-770, (2004).

10. Spalart, P. R. and Allmaras, S. R., A One-Equation Turbulence Model for Aerodynamic Flows, La Recherche Aerospatiale, 1, 5-21, (1994).
11. Ajmani, K., Kundu, K. and Penko, P.F., "A Study on Detonation of Jet-A Using a Reduced Mechanism," AIAA paper 2010-1515, January 2010.
12. Ajmani, K., Mongia, H.C. and Lee, P., "Evaluation of CFD Best Practices for Combustor Design: PART II – Reacting Flows", AIAA Paper 2013-1143, Jan. 2013.
13. Jachimowski, C.J., An Analytical Study of the Hydrogen-Air Reaction Mechanism with Application to Scramjet Combustion. NASA TP-2791, (1988).